NASA TECHNICAL NOTE

NASA TN D-7866

NASA TN D-7866

THE ANNULAR MOMENTUM CONTROL DEVICE (AMCD) AND POTENTIAL APPLICATIONS

Willard W. Anderson and Nelson J. Groom

Langley Research Center

Hampton, Va. 23665

NATIONAL AERONAUTICS AND SPACE ADMINISTRATION • WASHINGTON, D. C. • MARCH 1975

1. Report No.	2. Government Accession No.	3. Recipient's Catalog No.
NASA TN D-7866		

4. Title and Subtitle	5. Report Date
THE ANNULAR MOMENTUM CONTROL DEVICE (AMCD) AND POTENTIAL APPLICATIONS	March 1975
	6. Performing Organization Code
7. Author(s)	8. Performing Organization Report No.
Willard W. Anderson and Nelson J. Groom	L-9901
9. Performing Organization Name and Address	10. Work Unit No.
NASA Langley Research Center Hampton, Va. 23665	506-19-13-01
	11. Contract or Grant No.
12. Sponsoring Agency Name and Address	13. Type of Report and Period Covered
National Aeronautics and Space Administration Washington, D.C. 20546	Technical Note
	14. Sponsoring Agency Code

15. Supplementary Notes

16. Abstract

An annular momentum control device (AMCD) consisting principally of a spinning rim, a set of noncontacting magnetic bearings for supporting the rim, a noncontacting electric motor for driving the rim, and, for some applications, one or more gimbals is described. The device is intended for applications where requirements for control torque and momentum storage exist. Hardware requirements and potential unit configurations are discussed. Theoretical considerations for the "passive" use of the device are discussed. Potential applications of the device in other than passive configurations for the attitude control, stabilization, and maneuvering of spacecraft are reported.

17. Key Words (Suggested by Author(s))	18. Distribution Statement
Spacecraft stabilization Spacecraft control actuator Momentum storage device Control moment gyroscope	Unclassified – Unlimited STAR Category 31

19. Security Classif. (of this report)	20. Security Classif. (of this page)	21. No. of Pages	22. Price*
Unclassified	Unclassified	36	$3.75

*For sale by the National Technical Information Service, Springfield, Virginia 22151

THE ANNULAR MOMENTUM CONTROL DEVICE (AMCD) AND POTENTIAL APPLICATIONS

By Willard W. Anderson and Nelson J. Groom
Langley Research Center

SUMMARY

An annular momentum control device (AMCD) consisting principally of a spinning rim, a set of noncontacting magnetic bearings for supporting the rim, a noncontacting electric motor for driving the rim, and, for some applications, one or more gimbals is described. The device is intended for applications where requirements for control torque and momentum storage exist. Hardware requirements and potential unit configurations are discussed. Theoretical considerations for the "passive" use of the device are discussed. Potential applications of the device in other than passive configurations for the attitude control, stabilization, and maneuvering of spacecraft are reported.

INTRODUCTION

The use of stored angular momentum for the purpose of controlling the attitude of fine pointing or long duration spacecraft, where either environment contamination or excessive fuel use prohibit reaction jet usage, has become almost universal. Applications of the concept include spinning spacecraft (Tiros), dual-spin spacecraft (OSO), momentum wheel stabilized spacecraft (ITOS), reaction-wheel stabilized spacecraft (OAO), and, recently, the control moment gyroscope system used for stabilizing Skylab.

Each of these methods has advantages and disadvantages. Spinning the spacecraft (or a portion of it) to achieve attitude stability is simple and reliable, yet the spacecraft itself cannot be utilized fully because of its rotation. Also, any momentum axis reorientation maneuvers require external torques for momentum precession and the artificial gravity field produced may run counter to payload requirements for zero gravity. Stabilizing the spacecraft by utilizing a momentum wheel which provides gyroscopic stiffness equivalent to spinning the vehicle itself allows a nonspinning spacecraft and permits arbitrary orientations about the roll axis for the purpose of pointing onboard experiments. This technique does not overcome the inability to reorient or maneuver the spacecraft about all three axes without external torques since the spin axis of the momentum wheel is fixed with respect to the spacecraft. The use of three reaction wheels with axes alined with the spacecraft axes allows complete spacecraft active attitude control. However,

reaction-wheel momentum must be limited to relatively low amounts because of an excessive requirement for power when directly producing a torque on a rapidly spinning flywheel. The limitation on reaction-wheel momentum can be overcome by using a control moment gyro (CMG) system, which uses constant speed wheels and develops precession torques through controlled slewing of gimbaled flywheels. However, to achieve the smooth low-level torques necessary for fine pointing requires precise control of very low gimbal slew rates. These low gimbal rates are inherently limited by the requirement for high servo stiffness and thus high friction torque, unless extreme mechanical precision and resultant high cost are involved.

The purpose of this paper is to introduce a new development in the field of momentum storage devices, the annular momentum control device (AMCD).[1] The spinning assembly of the device is discussed in detail and its advantages relative to conventional flywheel design are presented. The use of the spin assembly as a momentum wheel ("passive" case) with spin axis control for spacecraft with orientation requirements such as those of Tiros, ITOS, or TACSAT is described in detail.

The use of the device for active pointing control, maneuvering, and other applications of spacecraft and experiment control is discussed in general terms. Emphasis is placed on the use of the device in applications where a large radius is allowable and beneficial since those applications are new. The device can be used as the spin assembly for any of the conventional momentum storage devices including reaction wheels and control moment gyros.

SYMBOLS

Values are given in both SI and U.S. Customary Units. The measurements and calculations were made in U.S. Customary Units.

A	rim cross-sectional area
E	transformation matrix
F	magnetic bearing forces
G	external torques
H	angular momentum

[1]Patent pending for "Annular Momentum Control Device," NASA Case No. LAR 11051-1.

H_a	total angular momentum of AMCD
H_S	spacecraft total angular momentum
I	moment of inertia
I_a	transverse AMCD rim inertia
I_S	transverse spacecraft inertia
Im( )	imaginary part of complex root
K_ℓ	magnetic bearing linear displacement gain
$K_{\dot{\ell}}$	magnetic bearing linear rate gain
K_S	flywheel energy shape factor (see eq. (A1))
K'_S	flywheel momentum shape factor (see eq. (1))
K_λ	magnetic bearing angular displacement gain
$K_{\dot{\lambda}}$	magnetic bearing angular rate gain
k	radius of gyration
m	mass
Re( )	real part of complex root
r	radius
s	distance along rim; also, Laplace operator
T	interaction torque
T_R	flywheel energy
t	time

v	arbitrary vector
X,Y,Z	coordinate axes
Y	Young's modulus
α	telescope azimuth
β	telescope elevation
γ	angle between axis of rotation and X-axis (see eqs. (C14))
δ	spacecraft rotation angle
ϵ_H	spin momentum ratio, H_s/H_a
ϵ_I	transverse inertia ratio, I_a/I_s
η	rim vibration amplitude
θ	transformation angle, Y-axis rotation angle
λ	rim rotation angle about axis of rotation (see eqs. (C14))
ξ	rim rotation angle
ρ	mass density
$(\rho_{syst})_{max}$	maximum system damping (see eq. (12))
ρ_∞	damping coefficient
σ	working stress
τ	magnetic bearing gain ratio, $K_{\dot{\lambda}}/K_\lambda$
ϕ	X-axis rotation

Ω_p uncoupled rim precessional frequency

ω angular velocity

ω' angular velocity cross product matrix

ω_f rim fundamental frequency

ω_H approximate precession frequency, $(H_a + H_s)/(I_a + I_s)$

ω_∞ stiffness factor, $(K_\lambda/I_s)^{1/2}$

Subscripts:

a AMCD rim

b body

d damped

f body fixed

i inertial

s spacecraft

T total

x,y,z coordinates

Superscripts:

c coordinate axes

-1 matrix inversion

* nondimensional with respect to ω_H

Dots over symbols denote derivatives with respect to time.

AMCD SPIN ASSEMBLY DESCRIPTION

The spin assemblies of momentum wheels, reaction wheels, and control moment gyroscopes used in attitude control systems for spacecraft to date have been of nearly conventional terrestrial design (shaft-driven steel flywheels with ball bearings). The AMCD spin assembly configuration is based on space usage (vacuum and zero gravity) and consists of a rotating rim (no central hub) suspended by noncontacting magnetic bearings and powered by a noncontacting linear electromagnetic motor. (See fig. 1.)

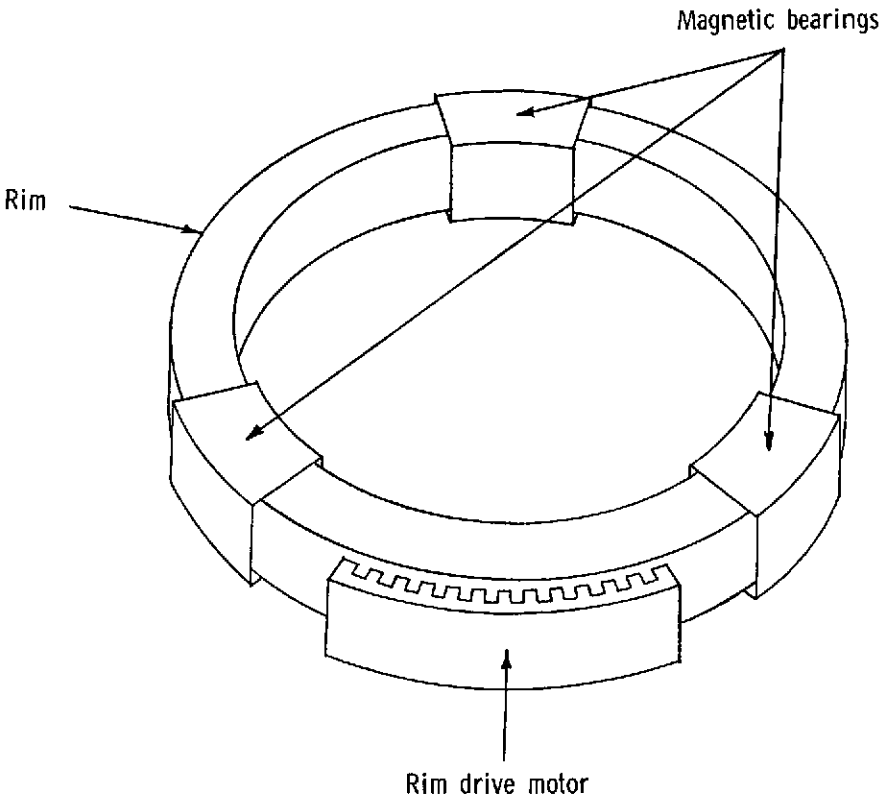

Figure 1.- Basic AMCD configuration.

The choice of configuration is based on several factors. The first factor is a desire to obtain maximum angular momentum for a given flywheel mass. The relationship of these two variables is discussed in appendix A (eq. (A3)) and is given as follows:

$$\frac{H}{m} = k\left(2K_S \frac{\sigma}{\rho}\right)^{1/2}$$

where H is the angular momentum, m the mass, k the radius of gyration, K_S a dimensionless shape factor, σ the allowable working stress, and ρ the density of the flywheel. A consideration when optimizing H/m is the specific stress σ/ρ of the material. From reference 1, working values of the square root of specific stress for

conventional metals (steels and aluminums) lie below 350 m/sec (1150 ft/sec), the stronger maraging steels approaching 500 m/sec (1640 ft/sec). Values of specific stress for the filaments of the stronger composite materials range from 1060 m/sec (3480 ft/sec) for boron and graphite to 1230 m/sec (4050 ft/sec) for the Dupont material PRD-49 (Kevlar). Clearly, from the aspect of specific stress, the composite materials are better. However, to achieve full utilization of the material strength requires a unidirectional layup of the composite.

Another consideration is the combined effect of size (radius of gyration) and shape. For a flywheel of constant shape, H/m is proportional to the radius of gyration k, and it is clear, therefore, that the largest possible k is optimum. However, flywheel size is normally limited by outside diameter and not by the radius of gyration. Equation (A3) is thus rewritten as

$$\frac{H}{m} = r_o\left(2K_S' \frac{g}{\rho}\right)^{1/2} \tag{1}$$

where r_o is the outside radius of the flywheel and

$$K_S' = K_S \frac{k^2}{r_o^2}$$

The maximum value for K_S' for the nine flywheel shapes considered in reference 2 is $K_S' = 0.500$ for the thin rim. It is interesting to note that not only is the thin rim an optimum flywheel shape but it is also one of the few flywheel shapes that will allow full utilization of the filament strengths of composite materials by allowing a unidirectional layup. This fact also makes the AMCD an attractive energy storage device.

The second factor behind the selection of the AMCD configuration is the multiple problems of wear, reliability, and vacuum lubrication of the ball bearings used in current and planned control moment gyros. To achieve the large momentum needed for Skylab and for planned shuttle and shuttle-launched missions requires flywheel speeds at values where ball bearing design is an empirical art necessitating extensive preflight testing of the bearings and lubrication system. As has been evidenced on Skylab, where two out of three of the control moment gyros developed bearing problems (one causing complete failure of the unit), poor performance can still result from this empirical design process. The use of magnetic bearings to support the rim eliminates all wear, requires no lubrication, and increases the reliability to that of the solid-state electronic bearing circuits.

A third factor is the isolation of the rotating rim from the spacecraft afforded by the magnetic bearings. Spacecraft vibration resulting from reaction wheel or CMG rotor unbalance and ball bearing element rotation can have a detrimental effect on the fine pointing of vehicles with high accuracy requirements such as the planned large space telescope. (See ref. 3.) Although imperfect balance of an AMCD rim would cause rim

motion, for the case of all active nonpermanent magnet bearings the motion itself would produce no disturbance on the spacecraft unless detected by the bearing sensors and then acted upon by the bearing force coils. For this reason, appropriate notch filtering at the spin frequency and at the fundamental vibrational frequency and possibly at the higher harmonics of both should eliminate vibrational input to the vehicle. It is interesting to note that for the thin-rim AMCD, it is not possible to have resonance between spin and spin plane vibration frequencies because the rim vibration frequencies, for the assumptions of appendix B, are always higher by a factor of at least two. Although the assumptions of appendix B do not cover all potential AMCD rim geometries, the equations illustrate the stiffening which occurs because of the tangential stress generated by rim rotation. Also this stiffening has the effect of circularizing the rim and improving balance at design speed.

A final factor to consider is the ability to command output torques for control usage directly with no mechanical or electrical breakout torque. This ability is implicit when the device is used either in the "passive" mode to be discussed later where control torques are generated by a damped centering of the rim between bearing elements or by direct command from spacecraft sensors when used in the "active" mode which is also discussed later.

AMCD SPIN ASSEMBLY HARDWARE CONSIDERATIONS

Because of its unique configuration, the AMCD presents several design constraints which interact with all components and result in basic requirements for any AMCD design. Obviously, any number of variations in the design of rim, motor, and/or bearings could be made in an attempt to better meet the specific design requirements for a given mission, but some general considerations warrant discussion.

Magnetic Bearing Considerations

For AMCD designs of large radial dimension, a very large weight penalty could occur if a continuous magnetic bearing around the rim was provided. In practical terms the total magnetic bearing structure weight could be two to three times that of the rim. This condition could compromise any system weight advantage presented by the AMCD design. The practical solution to the bearing problem is to use segmented bearings as shown in figure 1. The minimum number of bearing segments would be three with a variable number of elements per segment depending on particular design requirements.

Unfortunately, the use of segmented bearings to solve the bearing weight problem produces another potentially serious problem. Since the bearings are now in discrete sections, the rotating rim will see a discontinuous magnetic field. Unless proper choice

of rim design is made, this could result in appreciable eddy current and hysteresis power losses in the rim portion of the bearing magnetic circuit.

Rim Considerations

As mentioned previously, the use of segmented magnetic bearings introduces the design requirement that the rim portion of the bearing magnetic circuit have low eddy current and hysteresis losses. Thus, a low reluctance material with a very high resistivity and a narrow hysteresis loop is required. A material that has these characteristics in addition to the structural characteristics required for the rim structure does not currently exist. A practical solution to the conflicting rim material problem is to use a high-strength nonmagnetic and nonconducting composite material such as graphite epoxy for the rim structure and embed a low-loss magnetic material such as a ferrite material in the main rim structure to serve as the rim portion of the bearing magnetic circuit.

Rim Drive Motor Considerations

As with the magnetic bearings, the weight penalty for a motor stator that is continuous around the rim would be too high. Use of a linear motor employing one or more stator segments is one obvious solution. Again the problem of conflicting requirements for the rim material arises. As in the magnetic bearing solution, the rotor part of the motor magnetic circuit can be embedded in the main rim structure. For example, a permanent magnet dc brushless drive motor could be designed by utilizing permanent magnets embedded in the rim with a magnetic field detector to sense the position of a given magnet for commutation purposes.

AMCD Laboratory Model

An AMCD laboratory model embodying the design philosophy presented is being built for the Langley Research Center by Ball Brothers Research Corporation. The rim (fig. 2) is made of a graphite-epoxy composite, is 1.7 meters (5.5 feet) in diameter, weighs 222.4 N (50 pounds), and will rotate at 3000 rpm. The suspension system consists of three segments spaced equidistantly around the rim. Magnetic bearing elements at each segment interact with low-loss ferrite material embedded in the rim. The rim will be spun up by a series of stationary electromagnets that both push and pull on small samarium-cobalt permanent magnets also embedded in the rim.

THEORETICAL CONSIDERATIONS OF A "PASSIVE" AMCD-SPACECRAFT SYSTEM

The use of the AMCD as a "passive" device involves rigidly mounting the magnetic bearings and spin motor to the spacecraft and providing an active spacecraft control loop

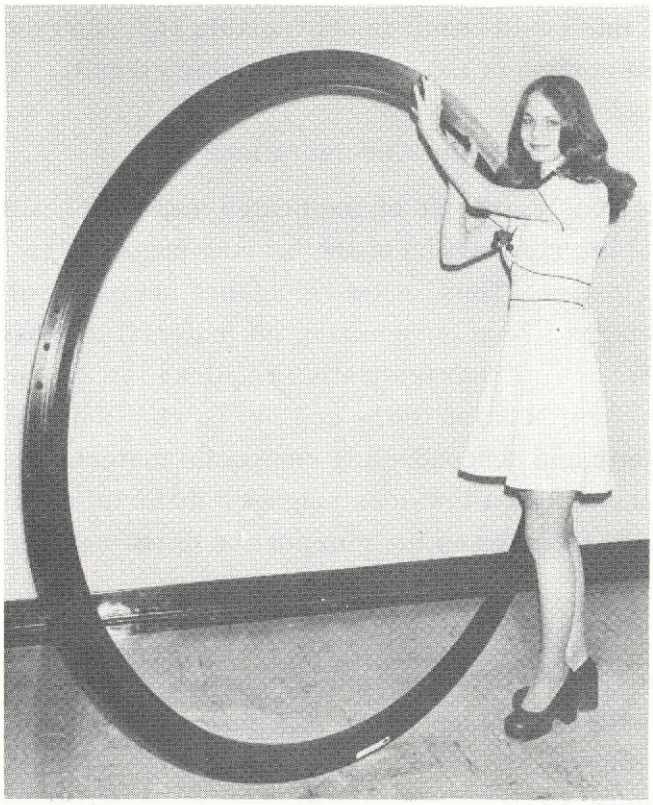

L-74-8547

Figure 2.- Graphite-epoxy rim for the AMCD laboratory model.

using spin motor torques for spacecraft roll or spin control. (See fig. 3.) The word passive is used because spacecraft sensors are not required for stabilization of spacecraft pitch and yaw axes although rim position sensors are required for the active magnetic bearings. Nonlinear and linearized equations of motion for the passive AMCD-spacecraft case are derived in appendix C. These equations were used to generate time histories and root locus plots which are discussed later. Before presenting these data, the rotational stability of the device is discussed.

Basic Rotational Stability Considerations

The linear model derived in appendix C does not contain spin axis torques when the AMCD spin motor torque is controlled to counteract AMCD rim friction (hysteresis and eddy current losses) since both the AMCD rim and the spacecraft are assumed to be symmetrical about the spin axis. This means that there is no mechanism within the model to allow the coning angle to increase since any increase in the coning angle can only be the result of a decrease in spin momentum if there are no external torques present.

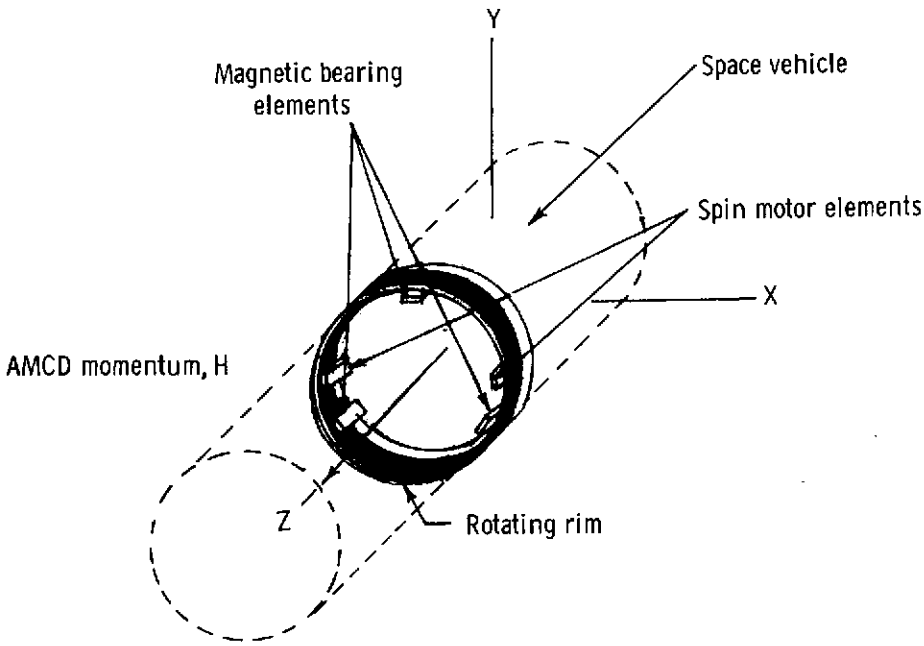

Figure 3.- "Passive" AMCD-spacecraft system.

To explain this further, assume that the relative transverse rotation between rim and spacecraft is small (as has been assumed throughout the report). Thus

$$H_T \cos \theta = I_{az}\omega_{az} + I_{sz}\omega_{sz} \tag{2}$$

where H_T is the total angular momentum of the system, θ is the angle between the Z-axis and the momentum vector, I_{az} and I_{sz} are the rim and spacecraft spin-axis moments of inertia, and ω_{az} and ω_{sz} are the spin rates of the rim and spacecraft. Differentiating with respect to time yields

$$\dot{\theta} = -\frac{I_{az}\dot{\omega}_{az} + I_{sz}\dot{\omega}_{sz}}{H_T \sin \theta} \tag{3}$$

and thus an increase in the cone angle θ is seen to require a net decrease in spin momentum. Obviously, if there are no spin axis torques acting directly on the two bodies and the two bodies are symmetrical about the spin axis (no spin-axis cross-coupling torques), the spin momentum is constant and therefore θ is constant.

In any real physical system, internal sources of energy dissipation do exist which can change the spin momentum. There are many references in the literature dealing with the subject of rotational stability based on models of dual-spin vehicles containing internal sources of energy dissipation which affect spin momentum. Vernon Landon (ref. 4) is credited with being the first investigator to explain the stability of dual-spin vehicles when these vehicles are not spinning about an axis of maximum inertia. For the purposes of this paper, it is assumed that the energy dissipation sources exist almost entirely within

the vehicle rather than within the AMCD rim. For this reason the requirement for rotational stability (for the case of small relative transverse rotations) reduces to a requirement that the rate of precession of the spin axis (Z-axis) about the total momentum vector be greater than the rate of spin of the spacecraft. (See ref. 5 for a mathematical derivation of this requirement.) For the passive AMCD-spacecraft system, this condition represents a minimum requirement for AMCD rim momentum which must be met to insure asymptotic rotational stabilities.

The linear model does contain terms which can render the system unstable. However, the instability would not affect the system cone angle, but rather would allow the relative transverse rotation between rim and spacecraft to increase in an unstable manner. These instabilities are examined after the characteristic equation for the linear model is discussed.

Characteristic Equation for the Linearized Model

The nonlinear and linearized equations of motion for the passive AMCD-spacecraft case are derived in appendix C. The nonlinear equations were used to generate time histories which are discussed later. The linearized set of equations (eqs. (C21)) has the following characteristic equation which will be used to discuss system behavior:

$$
\begin{aligned}
&s^2\Bigg(\left(\epsilon_I{}^2\right)s^6 + \left[2\tau\omega_\infty{}^2\epsilon_I\left(1+\epsilon_I\right)\right]s^5 + \left[2\omega_\infty{}^2\epsilon_I\left(1+\epsilon_I\right) + \tau^2\omega_\infty{}^4\left(1+\epsilon_I\right)^2 + \omega_H{}^2\left(\frac{1+\epsilon_I}{1+\epsilon_H}\right)^2\left(1+\epsilon_H{}^2\epsilon_I{}^2\right)\right]s^4 \\
&+ \left[2\tau\omega_\infty{}^4\left(1+\epsilon_I\right)^2 + 2\tau\omega_\infty{}^2\omega_H{}^2\left(\frac{1+\epsilon_I}{1+\epsilon_H}\right)^2\left(R\epsilon_H\,\frac{1+\epsilon_H\epsilon_I{}^2}{1+\epsilon_I} + 1 + \epsilon_H{}^2\epsilon_I\right)\right]s^3 + \Bigg\{\omega_\infty{}^4\left(1+\epsilon_I\right)^2 \\
&+ \tau^2\omega_\infty{}^4\omega_H{}^2\left(1+\epsilon_I\right)^2\left[1 + \left(\frac{R\epsilon_H}{1+\epsilon_H}\right)^2\right] + \left(\epsilon_H\omega_H{}^2\right)^2\left(\frac{1+\epsilon_I}{1+\epsilon_H}\right)^4 + 2\omega_\infty{}^2\omega_H{}^2\left(\frac{1+\epsilon_I}{1+\epsilon_H}\right)^2\left(1+\epsilon_H{}^2\epsilon_I\right)\Bigg\}s^2 \\
&+ \left[2\tau\omega_\infty{}^4\omega_H{}^2\left(1+\epsilon_I\right)^2 + 2\tau\omega_\infty{}^2\omega_H{}^4R\epsilon_H{}^2\left(\frac{1+\epsilon_I}{1+\epsilon_H}\right)^3\right]s + \left\{\omega_\infty{}^4\omega_H{}^2\left(1+\epsilon_I\right)^2\left[1 + \left(\tau\,\frac{R\omega_H\epsilon_H}{1+\epsilon_H}\right)^2\right]\right\}\Bigg) = 0
\end{aligned}
\tag{4}
$$

where

$$
\left.
\begin{aligned}
\tau &= \frac{K_\lambda'}{K_\lambda} & \epsilon_I &= \frac{I_a}{I_s} \\
\omega_\infty{}^2 &= \frac{K_\lambda}{I_s} & \epsilon_H &= \frac{H_s}{H_a} \\
\omega_H &= \frac{H_a + H_s}{I_a + I_s} & R &= \frac{I_a + I_s}{I_{sz}}
\end{aligned}
\right\}
\tag{5}
$$

and where K_λ and $K_{\dot\lambda}$ are the resultant angular and angular rate magnetic bearing constants, I_a and I_s are the AMCD rim and spacecraft transverse moments of inertia, and H_a and H_s are the AMCD rim and spacecraft spin momentums. (See appendix C.)

The coefficients of equation (4) were used to form a symbolic Routh stability array by means of a computerized symbolic manipulation routine called MACSYMA. An attempt to derive simplified conditions for system stability was not successful because of algebraic complexity. The stability of the system was then examined by using the method of reference 6. This examination yielded the following two conditions for stability for positive damping τ:

$$\frac{R\epsilon_H}{1+\epsilon_H} < 1$$

$$\left(\frac{\omega_\infty}{\omega_H}\right)^2 + \frac{1+\epsilon_I}{(1+\epsilon_H)^2}\left[1 - 2R\epsilon_H\frac{\epsilon_I}{1+\epsilon_I} + R\epsilon_H - \frac{1+\epsilon_H}{1+\epsilon_H(1-R)}\left(1 - R\epsilon_H\frac{\epsilon_I}{1+\epsilon_I}\right)^2 - \epsilon_H{}^2R^2\frac{\epsilon_I}{(1+\epsilon_I)^2}\right] > 0$$

These conditions agree numerically with the Routh array conditions.

It is informative to discuss simplified versions of equation (4) initially. For the case where the AMCD rim transverse inertia I_a and the spacecraft spin momentum H_S are relatively small (ϵ_I and $\epsilon_H - 0$), equation (4) simplifies to

$$s^2\left[\left(\tau^2\omega_\infty{}^4 + \omega_H{}^2\right)s^4 + \left(2\tau\omega_\infty{}^4 + 2\tau\omega_\infty{}^2\omega_H{}^2\right)s^3 + \left(\omega_\infty{}^4 + \tau^2\omega_\infty{}^4\omega_H{}^2 + 2\omega_\infty{}^2\omega_H{}^2\right)s^2\right.$$

$$\left. + \left(2\tau\omega_\infty{}^4\omega_H{}^2\right)s + \left(\omega_\infty{}^4\omega_H{}^2\right)\right] = 0 \qquad (6)$$

Referring to the first of equations (5), the variable τ is seen as a ratio of magnetic bearing gains or the required lead on the magnetic bearing rim displacement signal. (Also see eqs. (C17).) This variable defines system damping. Insight into the variable ω_∞ can be gained by letting the AMCD momentum become large ($\omega_H \to \infty$). Equation (6) is reduced to

$$s^2\left(s^2 + \tau\omega_\infty{}^2 s + \omega_\infty{}^2\right)^2 = 0 \qquad (7)$$

The combined behavior described by this equation is that of uncoupled X- and Y-axis vibration of the spacecraft (the two complex conjugate roots) with damped frequency

$$\omega_{\infty,d} = \omega_\infty\left(1 - \rho_\infty{}^2\right)^{1/2} \qquad \left(\rho_\infty < 1\right)$$

and damping coefficient

$$\rho_\infty = \frac{\tau\omega_\infty}{2}$$

and precession of the system (the two $s = 0$ roots) about the X- and Y-axes caused by external torques about the Y- and X-axis, respectively. Since the momentum is large for this case, the rate of precession (which is inversely proportional to momentum) would be zero in the limit as ω_H approached infinity.

The variable ω_H can be defined by allowing the control gain ratio or lead τ to approach infinity. Under this circumstance the AMCD rim is not allowed transverse motion with respect to the spacecraft; this situation is thus likened to a nonflexible dual-spin spacecraft. Equation (4) reduces to

$$s^2\left(s^2 + \dot{\delta}^2\right)\left(s^2 + \omega_H{}^2\right) = 0 \tag{8}$$

Thus, the variable ω_H is the frequency of the oscillatory mode of the system when no relative transverse motion is allowed. It is noted that the system has no damping when τ approaches infinity. Since the system obviously has no damping when τ is zero, the selection of the value of τ to maximize system damping is critical.

Figure 4 contains root locus plots for equation (6) with respect to a set of nondimensional variables,

$$\left.\begin{aligned} s^* &= \frac{s}{\omega_H} = Re^* + i\ Im^* \\ \tau^* &= \tau\omega_H \\ \omega_\infty^* &= \frac{\omega_\infty}{\omega_H} \end{aligned}\right\} \tag{9}$$

This relation allows a single figure representation, and also from practical considerations ω_H is of the order one. Only the upper left quadrant of the s^* plane is presented, the lower quadrant being a mirror image. Values of $\omega_\infty^* = 1.0$, 1.5, and 2.0 and τ^* varying from zero to infinity were used to generate figure 4.

For no damping ($\tau^* = 0$), the two positive roots of equation (6) are

$$s_{1,2}^* = i\omega_\infty^*\left[\frac{\omega_\infty^{*2}}{2} + 1 \pm \omega_\infty^* \frac{\left(\omega_\infty^{*2} + 4\right)^{1/2}}{2}\right]^{1/2} \tag{10}$$

If the damping τ^* is increased, the root loci are seen to be approximately semicircular, the positive limiting roots defined by equation (8) for τ^* large being

$$s^* = 0,\ 0,\ i \tag{11}$$

This situation corresponds very nearly to that for a spin-stabilized, dual-spin-stabilized, or momentum-wheel-stabilized spacecraft and points out a major advantage of an AMCD "passively" stabilized spacecraft, namely, the introduction of system damping. The maximum value for this damping for the "system" mode (the root which approaches

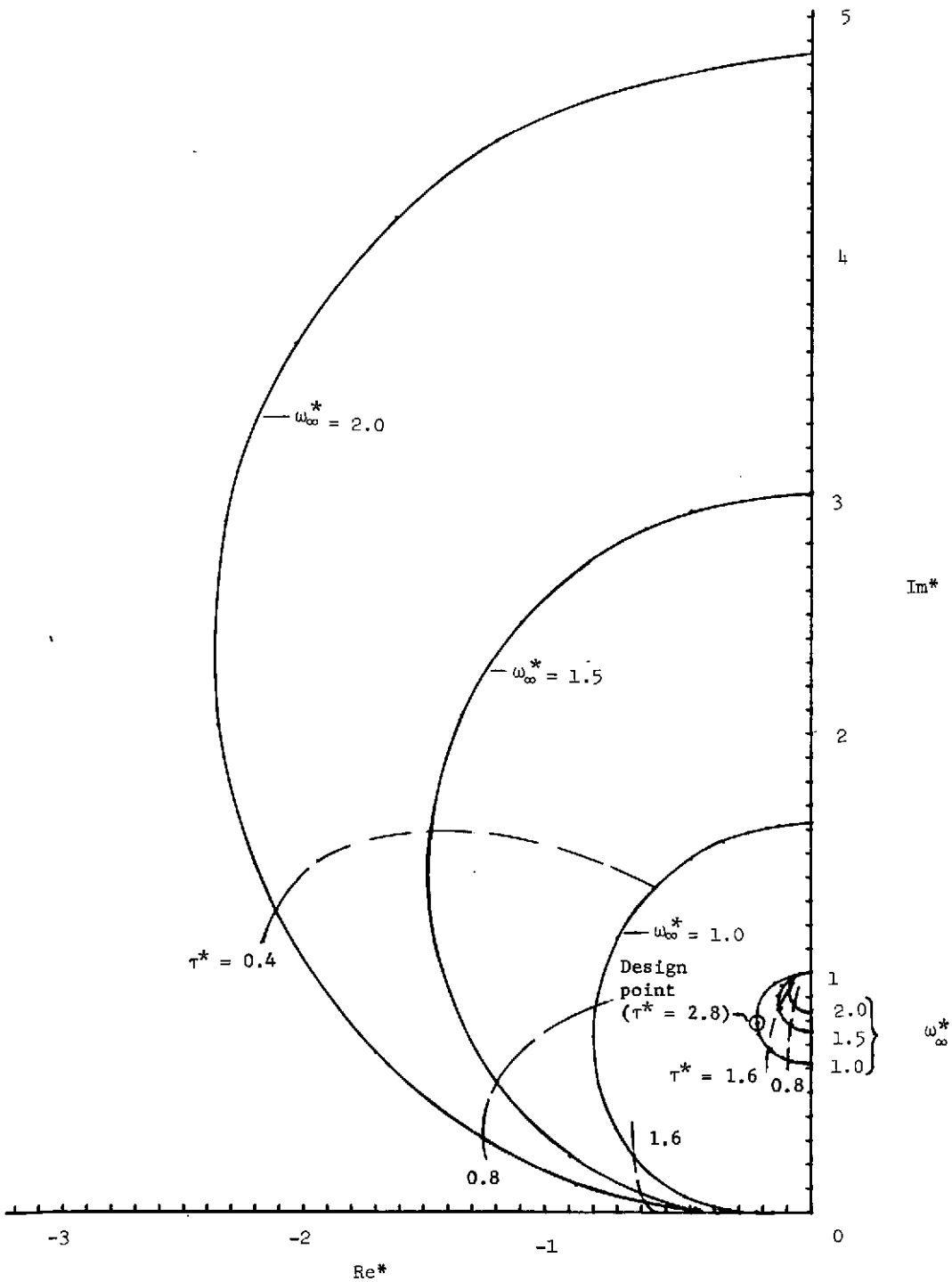

Figure 4.- Root locus of the basic "passive" system. $\epsilon_H = \epsilon_I = 0$.

$s^* = i$ or $s = i\omega_H$) which defines the "coning" motion associated with spin-stabilized spacecraft can be approximated by assuming the root locus to be semicircular. This assumption will yield

$$(\rho_{syst})_{max} = \frac{1 - |s_2^*|}{1 + |s_2^*|} \tag{12}$$

Although equation (12) predicts lower damping than that seen in figure 4, it is sufficient to illustrate trends. Figure 5 is a plot of $(\rho_{syst})_{max}$ determined from equation (12) for selected values of ω_∞ and ω_H. As can be seen from the figure, increasing the AMCD momentum (increasing ω_H) or decreasing the bearing stiffness (decreasing ω_∞) will allow higher maximum system damping.

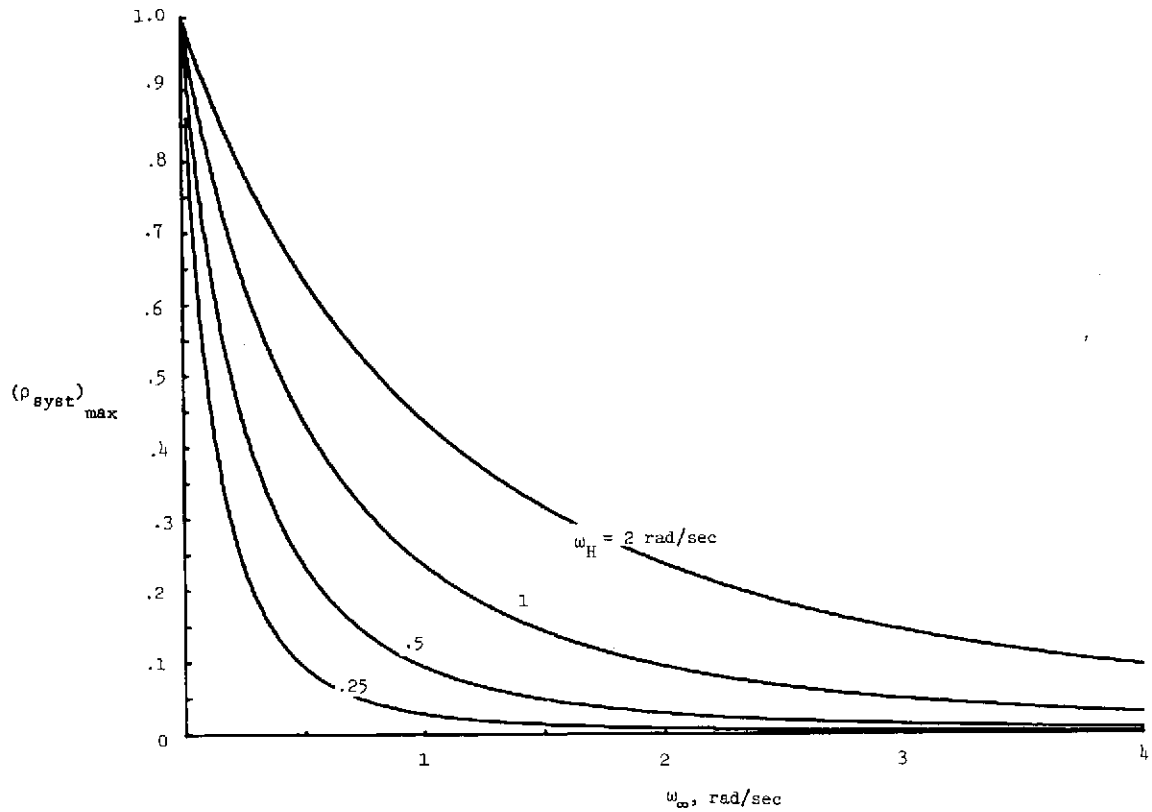

Figure 5.- System damping ratios.

From figure 5 it is seen that values of $(\rho_{syst})_{max}$ could theoretically be as high as one. However, from hardware considerations, there is a practical limit to the lead τ which must be taken into account in any specific design. An optimum selection of system damping has been accomplished which minimizes an integral absolute spacecraft pointing error criteria following an initial spacecraft offset. The value for the dimensionless variable τ^* based on these simulation runs is

$$\tau^* = 2.8$$

for a selected value of ω_∞^* of 1.0. This value of τ^* was independent of ω_H for the values of ω_H selected which varied from $\omega_H = 0.25$ to $\omega_H = 1.0$. This value is circled in figure 4 and can be used as a basis for an initial design of an AMCD "passive" system, provided ϵ_I and ϵ_H are negligible.

Spacecraft Rotation Effects

For some applications nonnegligible spacecraft rotation may be a requirement $(\epsilon_H \neq 0)$ and would occur, for example, for missions where Earth or satellite tracking was necessary. Figure 6 contains root locus plots for increasing τ^* for values of $\epsilon_H = 0$, 0.25, and 0.5; $\omega_\infty^* = 1.0$; $R = 2$; and $\epsilon_I = 0$. Since the variables plotted are normalized with respect to ω_H, the plots can be considered to represent a system with fixed total momentum. Therefore, for a given vehicle, transferring momentum from the AMCD to the spacecraft for the case where the spacecraft and AMCD rotate in similar directions $(\epsilon_H > 0)$ can be represented by loci of roots of constant τ^* and increasing ϵ_H. The "system" root exhibits decreased damping resulting from the decrease in AMCD momentum and this effect would require modification to these design criteria ($\tau^* = 2.8$).

Figure 7 contains root locus plots for increasing τ^* for values of $\epsilon_H = 0$, -0.1, and -0.15; $\omega_\infty^* = 1$; $R = 3$; and $\epsilon_I = 0$. Again, a given vehicle can be represented by loci of roots of fixed τ^* as ϵ_H increases negatively. The system root exhibits increased damping, resulting from increased AMCD momentum.

AMCD Inertia Effects

The AMCD rim has a basic precessional mode with an uncoupled frequency (for the thin rim assumption, $I_{az} = 2I_a$) of

$$\Omega_p = \frac{H_a}{I_a} = 2\dot{\xi}$$

Since the rim rotation rate $\dot{\xi}$ is large relative to other system frequencies, the effect of the rim precessional mode on the system roots has been found to be negligible; for example, in the generation of figures 4 to 7, no noticeable effect occurs when anticipated values of ϵ_I are included, and roots are found by use of equation (4). However, an additional complex root is found which represents rim precession, and which requires adequate magnetic bearing damping (proper selection of τ^*). Figure 8 contains plots of the damping ratio for this rim mode as a function of bearing lead τ^* for values of $\epsilon_H = -0.5$ to $\epsilon_H = 1.0$ and for a value of $\epsilon_I = 0.0025$ which results when nominal parameters are

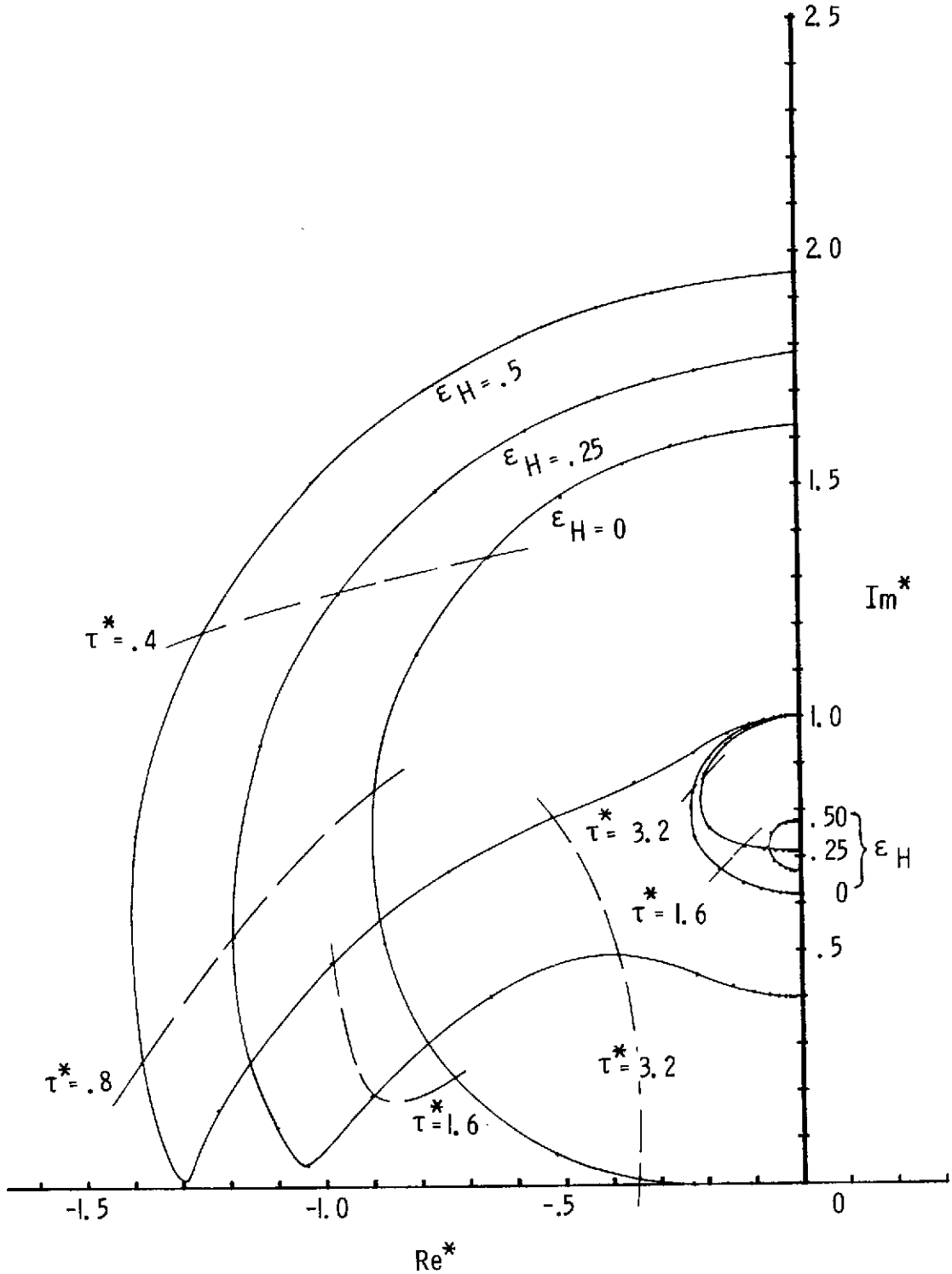

Figure 6.- Effects of positive spacecraft rotation. $\epsilon_I = 0$; $\omega^*_\infty = 1$; $R = 2$.

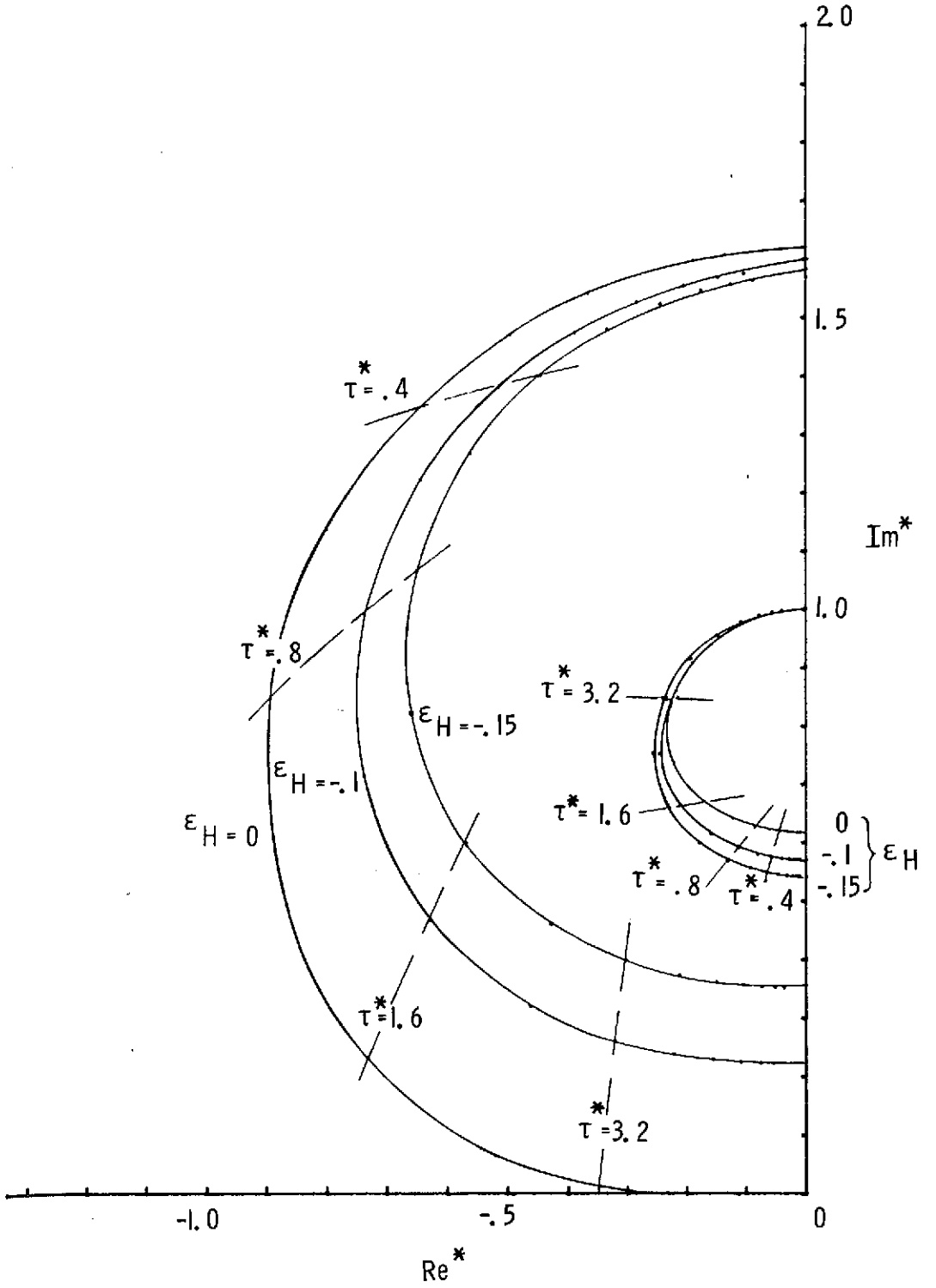

Figure 7.- Effects of negative spacecraft rotation. $\epsilon_I = 0$; $\omega^*_\infty = 1$; R = 2.

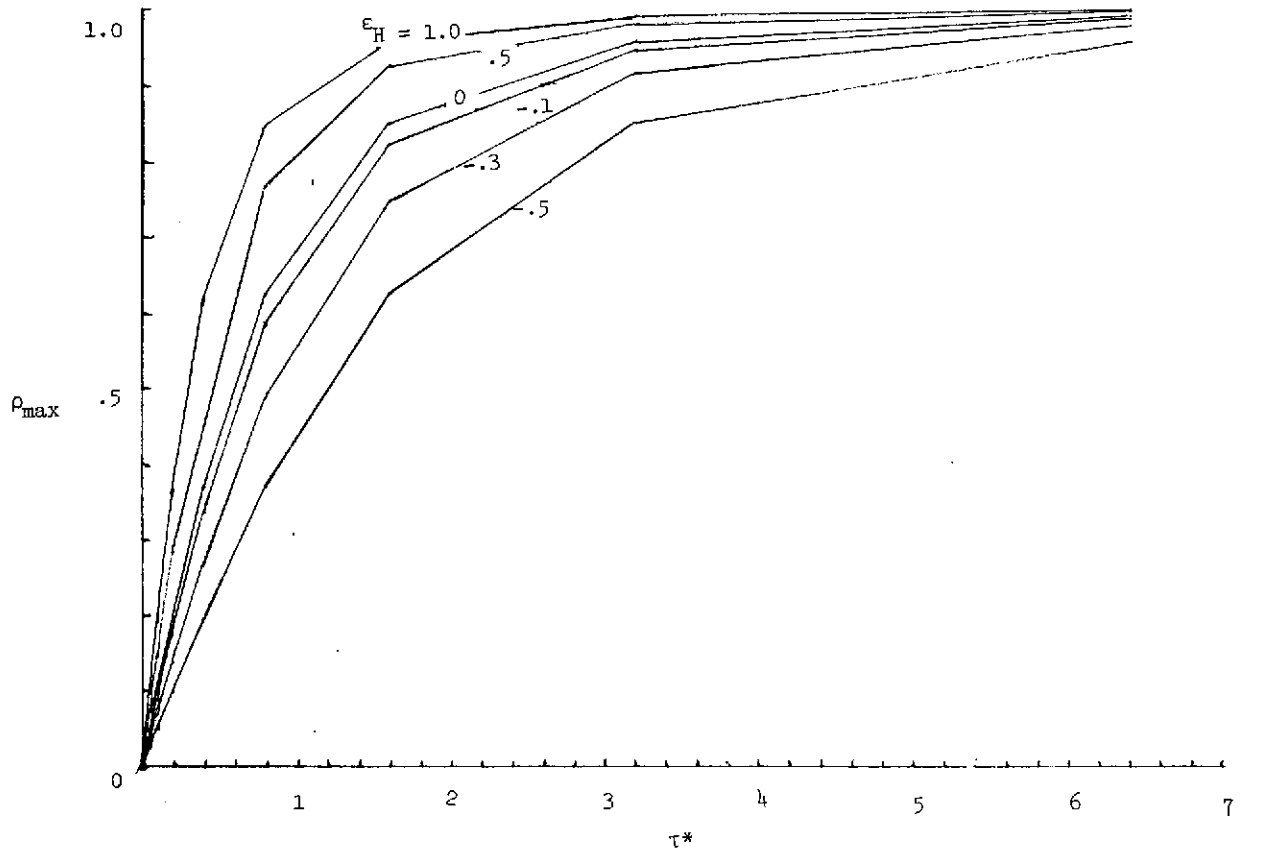

Figure 8.- Rim damping ratios. $\epsilon_I = 0.0025$.

selected. Values of the damped natural frequency of this mode did not vary significantly from the uncoupled precessional frequency Ω_p.

Simulation Results and Discussion

The nonlinear equations of motion for a passive AMCD-spacecraft configuration, which are derived in appendix C, were used to provide the time histories presented in this section. The spacecraft that was simulated does not represent a particular vehicle but should be representative of a typical Earth observation satellite. The configuration is basically a right circular cylinder with a diameter of 1.52 meters (5 feet), a length of 2.5 meters (8.2 feet), and a mass of 1175 kilograms (80.5 slugs). The transverse inertias are 680 kg-m^2 (500 slug-ft^2). An experiment-induced disturbance was used to illustrate the short-term dynamics of the system. The disturbances, shown in figure 9, represent the operation of protective doors and were taken from reference 7 (p. IX-17). The AMCD parameters were derived by assuming a thin-rim configuration with a diameter of 1.52 meters (5 feet) and a tip speed of 305 m/sec (1000 ft/sec). The parameters for the magnetic bearings (that is, stiffness and rate gain) were derived from the information

presented in figure 4 for ω_H and ω_∞^* of 1. From equations (5), since ϵ_I and ϵ_H approach 0, the momentum H_a of the AMCD is equal to the transverse inertia I_S of the spacecraft. From equations (9) (with $\omega_H = 1$), $\tau^* = \tau$ and $\omega_\infty^* = \omega_\infty$. By using the expression for ω_∞^2 in equations (5), the magnetic bearing stiffness K_ℓ was found to be 7.78 N/cm (4.44 lb/in.). The τ^* for optimum system damping, as indicated in figure 4, is 2.8. For purposes of illustration, one value of τ^* above and one value below the τ^* for optimum damping were included in the simulation. These values were 6.4 and 0.8, respectively.

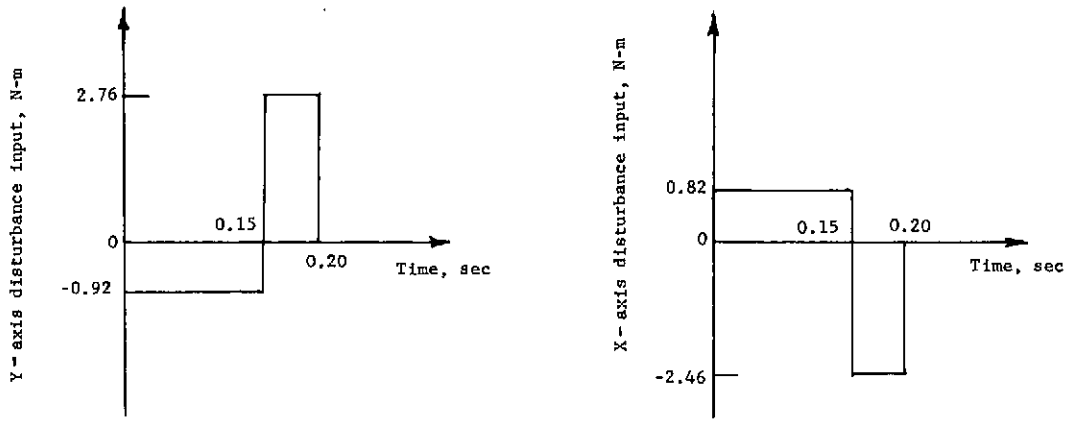

Figure 9.- Experiment disturbance torques.

The results of the simulation runs are presented in figures 10 to 14. Figures 10 to 12 represent a system with $\tau^* = 2.8$. Figures 10 and 11 show system pointing accuracy and damping characteristics. The system damping is very good, system motion being essentially damped out in approximately 3 cycles. Figure 12 is presented for the purpose of illustrating practical air gap requirements. It represents the motion of the rim center point within particular axial magnetic bearing segments so that the total peak-to-peak motion would represent the total bearing gap required to allow uninterrupted motion of the rim. The minimum bearing gap for the case considered is approximately 0.0012 cm (0.00047 in.). The bearing gaps would be made much larger than this in practice in order to ease machining tolerances. Figures 13 and 14 show system pointing accuracy and damping characteristics for τ^* of 0.8 and 6.4, respectively.

DESCRIPTION OF OTHER POTENTIAL USES OF AN AMCD

An "Active" AMCD-Spacecraft System

The use of an AMCD as an active device involves the generation of spacecraft torques in direct response to sensed spacecraft pointing errors. The torques would be generated by energizing the AMCD magnetic bearing flux coils in response to desired

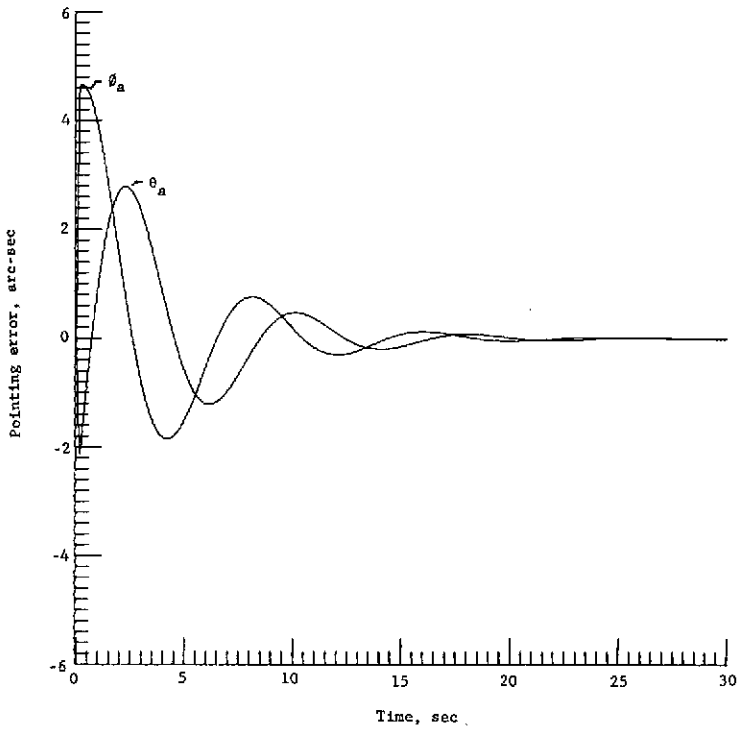

Figure 10.- Response of AMCD to disturbance input with $\omega_\infty^* = 1$ and $\tau^* = 2.8$.

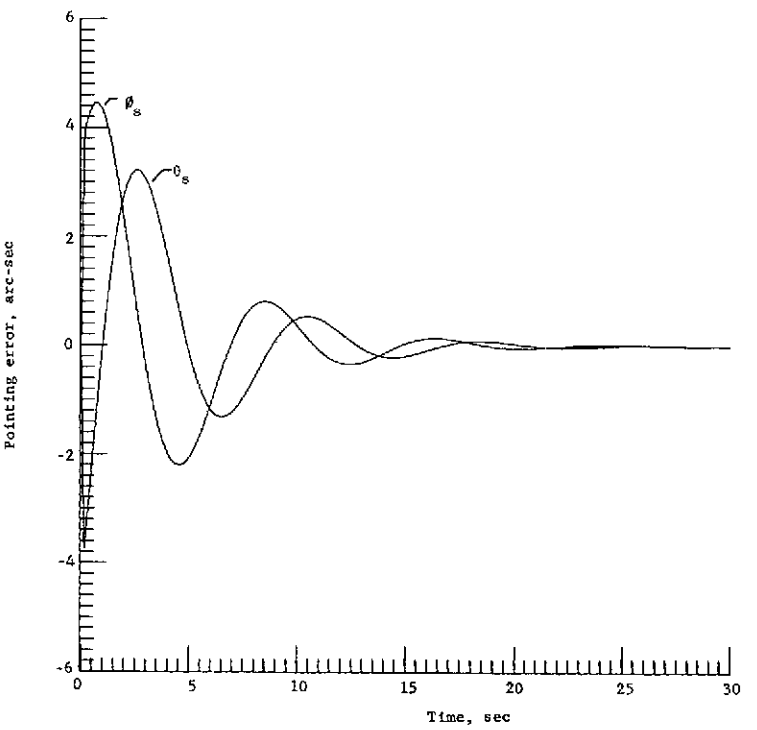

Figure 11.- Response of spacecraft to disturbance input with $\omega_\infty^* = 1$ and $\tau^* = 2.8$.

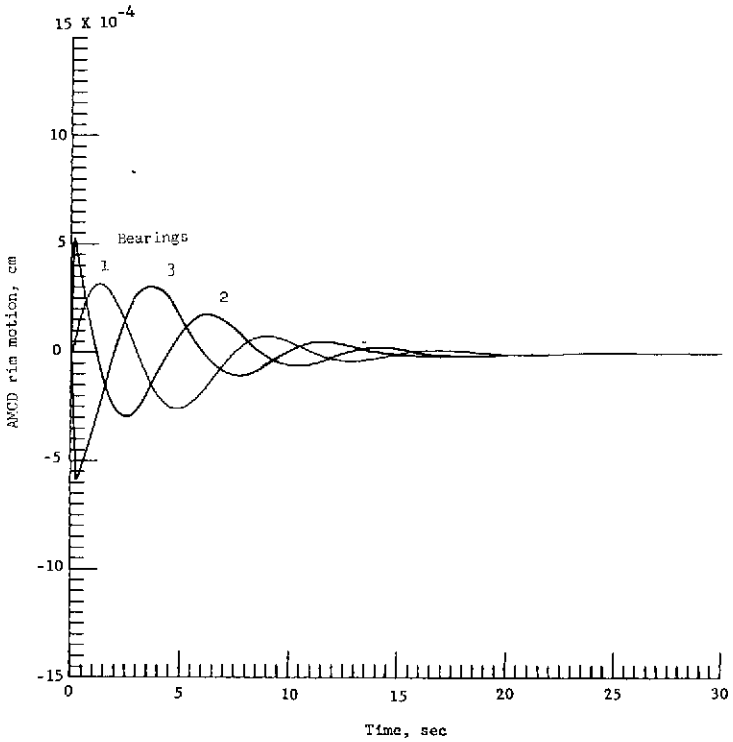

Figure 12.- AMCD rim motion in magnetic bearings with $\omega_{\infty}^{*} = 1$ and $\tau^{*} = 2.8$.

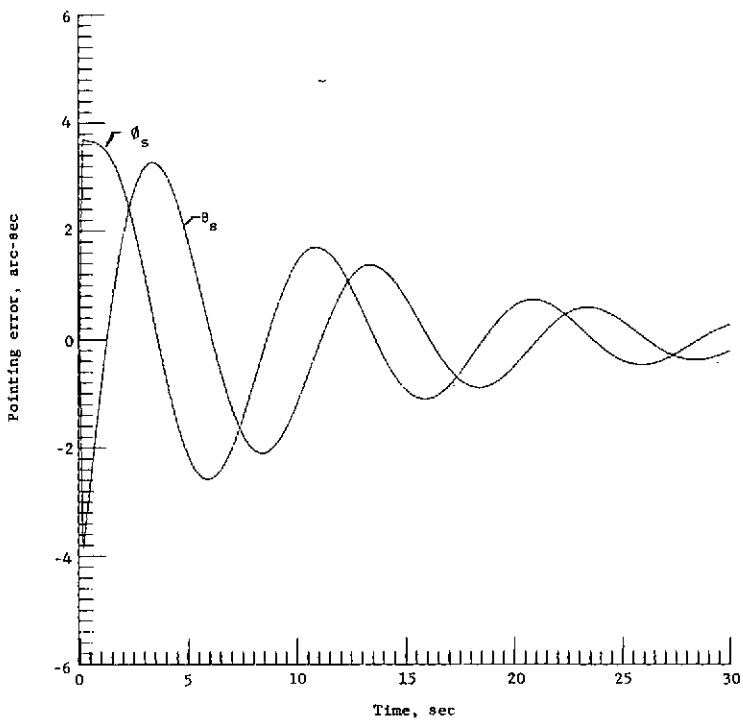

Figure 13.- Response of spacecraft to disturbance input with $\omega_{\infty}^{*} = 1$ and $\tau^{*} = 0.8$.

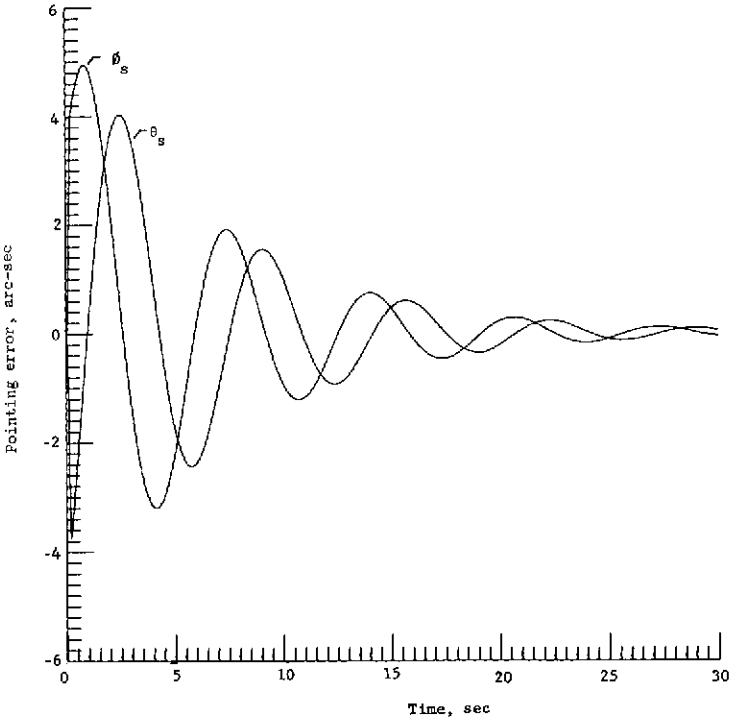

Figure 14.- Response of spacecraft to disturbance input with $\omega_\infty^* = 1$ and $\tau^* = 6.4$.

control torques based on spacecraft sensor outputs. The spacecraft is reoriented by producing torques against the AMCD rim momentum.

Two possible configurations of an active system are shown in figure 15. The spin-axis-pointing configuration of figure 15(a) allows both spacecraft pitch and yaw axes to be controlled by the magnetic bearing/torquers. However, if the target were the Earth or Sun, this configuration would require application of an external torque to precess the AMCD momentum vector at the appropriate rate. This configuration might be practical for solar viewing from Earth orbit (1^o per day precession) by producing torques against the Earth's magnetic field with the use of conventional flux coils. Figure 15(b) illustrates an alternative configuration in which the AMCD momentum vector is alined perpendicular to the orbit plane for Earth viewing and perpendicular to the ecliptic plane for solar viewing. This configuration allows complete spacecraft reorientation about the AMCD spin axis with no requirement for direct external torques, orbit regression being neglected. The second configuration does require that pointing control torques be generated about the spin axis; this was accomplished by using the spin motor with an inherent increase in required power. The pointing field of view in both cases is limited at least partially by the magnetic bearing gap and thus an additional mechanism is required for spacecraft maneuvering.

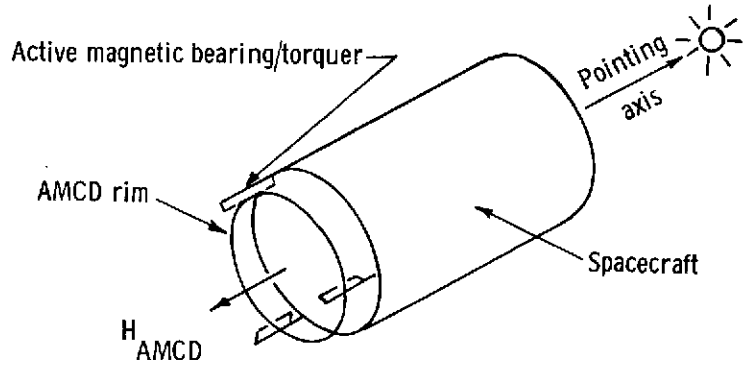

(a) Spin axis pointing.

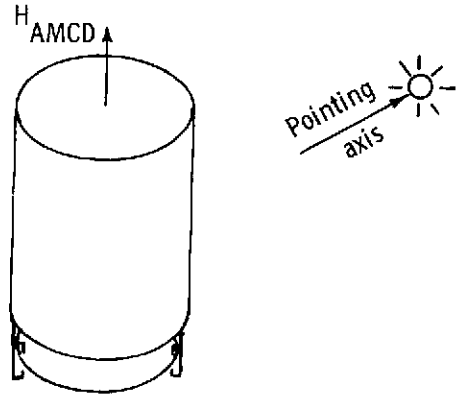

(b) Spin axis perpendicular to pointing axis.

Figure 15.- Active AMCD-spacecraft system.

AMCD-Spacecraft Maneuvering

Large angle spacecraft reorientation or maneuvering can be accomplished in a variety of ways by using one or more AMCDs; however, only the two ways which appear to be most practical for large radius AMCDs are discussed. In figure 16(a), a single-gimbal, single AMCD for arbitrary orientation of the pointing axis of a spacecraft is shown. By making an analogy with Earth-based telescopes, the azimuth angle α is generated by AMCD spin-axis control, and the elevation angle β is generated by producing torques against the AMCD momentum on the spacecraft by using a gimbal torquer(s). By limiting the spacecraft momentum during the maneuver to a small fraction of the AMCD momentum, one can see that the AMCD would remain nearly fixed, and the spacecraft would move in a fashion similar to that of an Earth-based telescope. When the spacecraft pointing axis is appropriately alined with the new target, the gimbal torquer would be locked in place and fine pointing would be accomplished by using the active technique discussed previously.

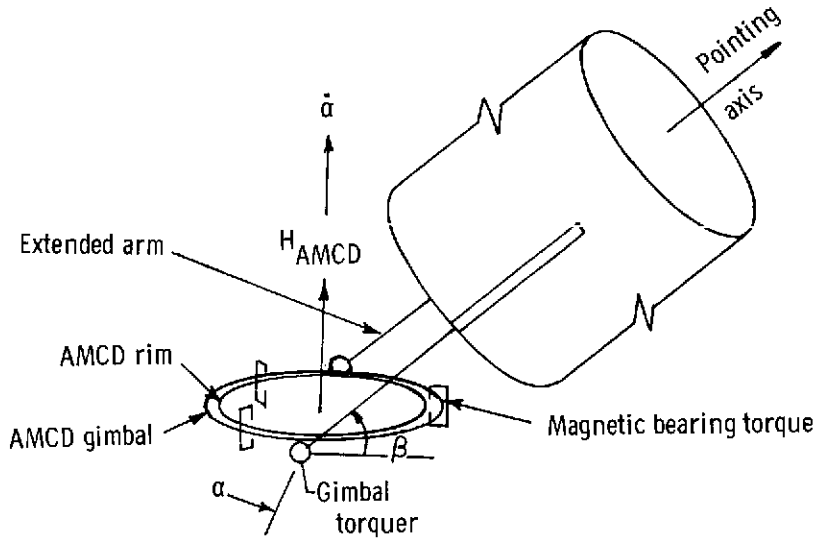

(a) Single-gimbal, single-AMCD maneuver configuration.

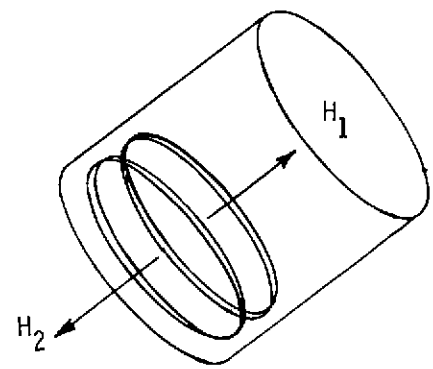

(b) Counterrotating AMCD pair configuration.

Figure 16.- Two AMCD-spacecraft maneuver configurations.

In figure 16(b) a second configuration is shown where two counterrotating AMCDs are shown mounted directly to a spacecraft. By reorienting the two rims within their respective magnetic bearing gaps or by using a limited gimbaling of one AMCD and also spinning up or despinning the rims, some momentum with appropriate direction can be imparted to the spacecraft. This momentum represents a maneuvering spacecraft with termination of the maneuver begun at a desired orientation. If all initial (prior to the maneuver) nonzero momentum can be accommodated by the two AMCDs at the new orientation, all spacecraft rates can be nulled. Thus, arbitrary maneuvers can be performed with this system if given sufficient magnetic bearing gap or gimbal freedom and spin speed range. Once the spacecraft has reached a new orientation, one or both of the AMCDs can be used in an active or passive mode for spacecraft pointing or stabilization. This configuration can also be used for combined power storage and control by maintain-

ing a net momentum difference between H_1 and H_2. The net momentum vector can stabilize the spacecraft in a passive manner as discussed previously, and power can be put into and taken from the system by spinning the two rims up or down while maintaining a fixed difference in rotational speed.

Additional Applications

The AMCD can be used as a vernier experiment pointing system by mounting the experiment to the rim and the magnetic bearing to the spacecraft (or vice versa) and providing vernier pointing torques with the magnetic bearings by using fine pointing information from the experiment package. The rim does not spin at high speed but the spin motor is required for roll orientation and control. The magnetic bearings produce torques against the spacecraft inertia and stabilization system rather than against the rim momentum.

Although this report has emphasized the large radius applications of the AMCD, the device may well be appropriate as the spin assembly for any conventional momentum storage device, such as a reaction wheel, control moment gyroscope, or the gyroscopic sensing systems found in aerospace vehicles.

CONCLUDING REMARKS

A device with potential broad application to spacecraft control and other momentum storage applications has been defined and considerations of its configuration and use discussed. Examination of the device as a momentum storage unit and system indicates the following advantages:

1. The rotating element approaches a thin rim which is the optimum shape for a given stress-limited material when maximizing momentum for a given mass of material and for a given maximum radius.

2. The thin rim allows a unidirectional filament layup of composites; thus, the maximum usage of these high strength-weight materials is allowed.

3. The configuration allows, where possible and desirable, the use of a large rim diameter with the inherent additional increase in momentum-mass ratio.

4. The noncontacting magnetic bearings and drive motor eliminate all mechanical friction and wear and should yield a device reliability equal to that of the solid-state electronic circuits.

5. The isolation of the rotating rim from the spacecraft affords an effective control over transmittal of rim vibration to the spacecraft when active magnetic bearings with no permanent magnetism are used. This is true because any forces transmitted to the

spacecraft would be the result of sensed rim motion and subsequent flux coil energizing, and would thus allow appropriate notch filtering in the electronics at spin and vibrational frequencies.

6. The magnetic bearings also provide the capability for directly producing torques on the spacecraft with no mechanical or electrical breakout torques involved.

7. For the "passive" mode of spacecraft control (when compared with single-spin, dual-spin, or gyrostat control), much improved precessional damping can be shown theoretically.

8. For the "passive" mode of spacecraft control, smaller attitude errors caused by environmental torques will result from the higher momentum allowed by the AMCD for a given momentum storage weight.

9. For the "active" mode of spacecraft control, extreme precision fine pointing is projected since extremely low spacecraft control torques can be easily generated with the magnetic bearings used as spacecraft torquers driven by spacecraft attitude sensors.

Finally, it is noted that the AMCD can be used as the spin assembly for any of the conventional momentum storage control devices (such as reaction wheels or control moment gyroscopes) with the unit characteristics of the AMCD offering the potential for significant improvements.

Langley Research Center,
National Aeronautics and Space Administration,
Hampton, Va., December 19, 1974.

APPENDIX A

FLYWHEEL MOMENTUM DENSITY

By considering the constraint on flywheel speed to be determined by allowable working stress, the specific energy of a flywheel can be determined from the relationship (ref. 2)

$$\frac{T_R}{m} = K_S \frac{\sigma}{\rho} \tag{A1}$$

where T_R is the stored kinetic energy; m, the mass; K_S, a dimensionless flywheel shape factor; σ, the design working stress; and ρ, the material density.

This relationship (eq. (A1)) can be modified to yield the specific momentum of a flywheel by noting that

$$\left.\begin{aligned} T_R &= \frac{H\omega}{2} \\ H &= mk^2\omega \end{aligned}\right\} \tag{A2}$$

where H is the angular momentum; ω, the angular velocity; and k, the radius of gyration of the flywheel.

Substitution of equations (A2) into equation (A1) yields

$$\frac{H}{m} = k\left(2K_S \frac{\sigma}{\rho}\right)^{1/2} \tag{A3}$$

Shape factors for homogeneous materials are given in reference 2 for nine different flywheel geometries and vary from 0.305 for a flat pierced disk to a theoretical limit of 1.000 for a constant-stress disk with an outer diameter approaching infinity. The shape factor for a thin rim is 0.500. A factor of 0.85 represents a practical limit.

APPENDIX B

AMCD STIFFNESS EFFECTS

The equation of motion for AMCD rim vibrations in the spin plane is assumed to be that of a rod under tension with rim thickness negligible when compared with rim radius. The equation, from reference 8, is

$$\sigma A \frac{\partial^2 \eta}{\partial s^2} - YI \frac{\partial^4 \eta}{\partial s^4} = \rho A \frac{\partial^2 \eta}{\partial t^2} \tag{B1}$$

where σ is the tangential stress; A, the cross-sectional area; Y, Young's modulus; I, the area moment of inertia; ρ, the density of the rim; η, the amplitude of in-plane vibration; and s, the distance along the rim. The frequency of the fundamental mode can be found from the following solution to equation (B1):

$$\eta = \eta_o \sin\left(2 \frac{s}{r}\right) \sin \omega_f t \tag{B2}$$

where η_o is an arbitrary constant. Also it is noted that $\sigma = \rho r^2 \omega^2$ for a thin rim, where ω is the spin frequency.

Substituting equation (B2) into equation (B1) and simplifying yields the relationship

$$\omega_f = \sqrt{(2\omega)^2 + \omega_{f,o}^2} \tag{B3}$$

where

$$\omega_{f,o} = \frac{4}{r^2}\sqrt{\frac{YI}{\rho A}} \tag{B4}$$

From equation (B3) it can be seen that the vibration frequency ω_f is always at least twice as great as the spin frequency ω. This formulation neglects rim inextensibility for the sake of simplicity.

APPENDIX C

DERIVATION OF "PASSIVE" AMCD-SPACECRAFT EQUATIONS OF MOTION

The derivation begins by considering Euler's equations of motion in matrix notation for an arbitrary rigid body written with respect to a set of axes fixed to the body,

$$T_b = I_b\dot{\omega}_b + \omega_b' H_b \tag{C1}$$

where T_b are the external torques; I_b, the inertia matrix; ω_b', the body rates of rotation written as a cross product matrix; and H_b, the angular momentum. This body represents the rotating rim of the AMCD.

Since the magnetic bearings which produce the torques T_b are fixed to the spacecraft, it is required to transform equation (C1) to a second arbitrarily oriented axis system. This transformation E_{ab} is defined by the equation

$$v_a = E_{ab}v_b \tag{C2}$$

where v_a and v_b are arbitrary vectors.

The transformation of equation (C1) begins by multiplying both sides by E_{ab} and by substituting, as indicated, the unity matrix taken as $E_{ab}^{-1}E_{ab}$. This procedure yields

$$E_{ab}T_b = E_{ab}I_bE_{ab}^{-1}E_{ab}\dot{\omega}_b + E_{ab}\omega_b'E_{ab}^{-1}E_{ab}H_b \tag{C3}$$

Equation (C3) can be simplified by defining

$$\left.\begin{aligned} T_a &= E_{ab}T_b \\ I_a &= E_{ab}I_bE_{ab}^{-1} \\ H_a &= E_{ab}H_b \\ \omega_a' &= E_{ab}\omega_b'E_{ab}^{-1} \qquad \text{(matrix)} \\ \omega_a &= E_{ab}\omega_b \qquad \text{(vector)} \end{aligned}\right\} \tag{C4}$$

By differentiating the last of equations (C4), it is seen that

$$\left.\begin{aligned} \dot{\omega}_a &= E_{ab}\dot{\omega}_b + \dot{E}_{ab}\omega_b \\ E_{ab}\dot{\omega}_b &= \dot{\omega}_a - \dot{E}_{ab}\omega_b \end{aligned}\right\} \tag{C5}$$

Substituting equations (C4) and (C5) into equation (C3) yields

$$T_a = I_a\dot{\omega}_a + \omega_a'H_a - I_a\dot{E}_{ab}E_{ab}^{-1}\omega_a \tag{C6}$$

By assuming the a-coordinate system and the b-coordinate system to have the same Z-axis, with a rotation of ξ about the Z-axis of the b-coordinate system relative to the a-coordinate system,

$$\underline{E}_{ab} = \begin{bmatrix} \cos\xi & -\sin\xi & 0 \\ \sin\xi & \cos\xi & 0 \\ 0 & 0 & 1 \end{bmatrix} \tag{C7}$$

Equation (C6) can now be expanded and, by assuming AMCD rim symmetry ($I_{bx} = I_{by} = I_a$), becomes

$$\left.\begin{aligned} T_{ax} &= I_a\dot{\omega}_{ax} + (I_{az} - I_a)\omega_{ay}\omega_{az} + \dot{\xi}I_a\omega_{ay} \\ T_{ay} &= I_a\dot{\omega}_{ay} + (I_a - I_{az})\omega_{ax}\omega_{az} - \dot{\xi}I_a\omega_{ax} \\ T_{az} &= I_{az}\dot{\omega}_{az} \end{aligned}\right\} \tag{C8}$$

Equations (C8) can now be modified to separate the effect of the large AMCD rim spin velocity by introducing the variable ω^c_{az} which will represent the angular velocity of the a-coordinate system about the Z-axis where

$$\omega_{az} = \omega^c_{az} + \dot{\xi} \tag{C9}$$

Equations (C8) now become

$$\left.\begin{aligned} T_{ax} &= I_a\dot{\omega}_{ax} + (I_{az} - I_a)\omega_{ay}\omega^c_{az} + I_{az}\dot{\xi}\omega_{ay} \\ T_{ay} &= I_a\dot{\omega}_{ay} + (I_a - I_{az})\omega^c_{az}\omega_{ax} - I_{az}\dot{\xi}\omega_{ax} \\ T_{az} &= I_{az}\dot{\omega}^c_{az} + I_{az}\ddot{\xi} \end{aligned}\right\} \tag{C10}$$

These equations are the equations of motion of the AMCD rim written in the a-system.

A second set of Euler's equations for the spacecraft is now introduced, where the algebra of the transformation of axes is omitted and where the AMCD and spacecraft centers of mass are assumed to be coincident,

$$\left.\begin{aligned} G_x + T_{sx} &= I_s\dot{\omega}_{sx} + (I_{sz} - I_s)\omega_{sy}\omega^c_{sz} + I_{sz}\dot{\delta}\omega_{sy} \\ G_y + T_{sy} &= I_s\dot{\omega}_{sy} + (I_s - I_{az})\omega^c_{sz}\omega_{sx} - I_{sz}\dot{\delta}\omega_{sx} \\ G_z + T_{sz} &= I_{sz}\dot{\omega}^c_{sz} + I_{sz}\ddot{\delta} \end{aligned}\right\} \tag{C11}$$

where G is an external disturbance torque, spacecraft symmetry is assumed ($I_{sx} = I_{sy} = I_s$), and $\omega_{sz} = \omega^c_{sz} + \dot{\delta}$. These equations are written in the s-system.

The rates ω_{az}^{c} and ω_{sz}^{c} are set equal to zero and the a- and s-coordinate axes are assumed to be nearly coincident except for small transverse relative rotations. This procedure allows a simplification in the calculation of the interaction torques by introducing a transformation matrix from the s-coordinate system to the a-coordinate system as follows:

$$E_{as} = E_{ai}E_{is} = E_2(\theta_a)\, E_1(\phi_a)\left[E_2(\theta_s)\, E_1(\phi_s)\right]^{-1} = E_2(\theta_a)\, E_1(\phi_a)\, E_1^{-1}(\phi_s)\, E_2^{-1}(\theta_s)$$

$$= E_2(\theta_a)\, E_1(\phi_a)\, E_1(-\phi_s)\, E_2(-\theta_s) = E_2(\theta_a)\, E_1(\phi_a - \phi_s)\, E_2(-\theta_s) \qquad \text{(C12)}$$

where the subscript i is introduced to represent an inertial reference and the notation $E_j(\,)$, j = 1 and 2, refers to a transformation from one coordinate system to another which has been rotated through an angle denoted by ( ) about an axis j. The Euler angles chosen to represent the positions of the a- and s-coordinate axes with respect to an inertial axis set are ϕ and θ with a 1,2 rotation sequence (x,y) selected.

By expanding the matrices in equation (C12) for the case when $\phi_a - \phi_s$, θ_a, and θ_s are small, the following equation is found to hold:

$$E_{as} \doteq E_2(\theta_a - \theta_s)\, E_1(\phi_a - \phi_s) \doteq E_1(\phi_a - \phi_s)\, E_2(\theta_a - \theta_s) \qquad \text{(C13)}$$

Because of the small angles $(\phi_a - \phi_s)$ and $(\theta_a - \theta_s)$, Euler's theorem on rotations can be used to show that

$$\lambda = \left[(\phi_a - \phi_s)^2 + (\theta_a - \theta_s)^2\right]^{1/2}$$

$$\sin i = \frac{\theta_a - \theta_s}{\lambda}$$

$$\cos i = \frac{\phi_a - \phi_s}{\lambda}$$

$$\frac{di}{dt} = \frac{(\dot{\theta}_a - \dot{\theta}_s)\cos i - (\phi_a - \phi_s)\sin i}{\lambda}$$

where the second set of Euler angles λ and i is shown in figure 17.

The torques on the AMCD rim resulting from "passive" or centering-only magnetic bearing forces F_1, F_2, and F_3 (see fig. 17) can be expressed as a function of the rotation λ and the angle γ and the linear magnetic bearing gains K_ℓ and $K_{\dot{\ell}}$ as follows. The bearing forces acting on the rim are defined by

$$\left.\begin{aligned} F_1 &= \left(K_\ell\lambda + K_{\dot{\ell}}\dot{\lambda}\right)r \sin\gamma + K_{\dot{\ell}}\lambda r\dot{\gamma}\cos\gamma \\ F_2 &= -\left(K_\ell\lambda + K_{\dot{\ell}}\dot{\lambda}\right)r \sin(60^\circ + \gamma) - K_{\dot{\ell}}\lambda r\dot{\gamma}\cos(60^\circ + \gamma) \\ F_3 &= \left(K_\ell\lambda + K_{\dot{\ell}}\dot{\lambda}\right)r \sin(60^\circ - \gamma) - K_{\dot{\ell}}\lambda r\dot{\gamma}\cos(60^\circ - \gamma) \end{aligned}\right\} \qquad \text{(C14)}$$

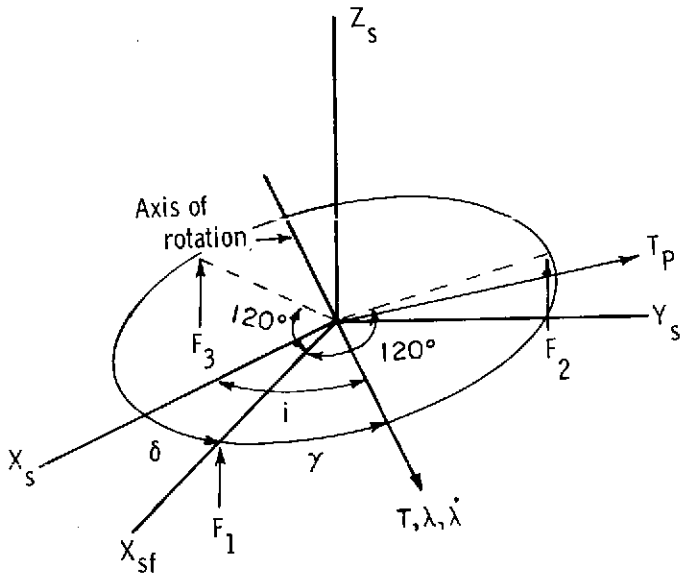

Figure 17.- Magnetic bearing forces and resultant torque.

where γ is shown in figure 17. The sum of F_1, F_2, and F_3 is zero. The forces are assumed to act perpendicular to the rim.

The torque is the resultant of the individual torques produced by the bearing forces

$$\left.\begin{aligned} T &= \left[-F_1 \sin\gamma + F_2 \sin(60^\circ + \gamma) - F_3 \sin(60^\circ - \gamma)\right] r \\ T_P &= \left[-F_1 \cos\gamma + F_2 \cos(60^\circ + \gamma) + F_3 \cos(60^\circ - \gamma)\right] r \end{aligned}\right\} \quad \text{(C15)}$$

Substituting equations (C14) into equations (C15) and simplifying yields

$$\left.\begin{aligned} T &= -K_\lambda \lambda - K_{\dot\lambda} \dot\lambda \\ T_P &= -K_{\dot\lambda} \lambda \dot\gamma \end{aligned}\right\} \quad \text{(C16)}$$

where

$$\left.\begin{aligned} K_\lambda &= 1.5 r^2 K_\ell \\ K_{\dot\lambda} &= 1.5 r^2 K_{\dot\ell} \end{aligned}\right\} \quad \text{(C17)}$$

Thus, for the case of 120° spacing, the net bearing torque is not dependent on the position of the magnetic bearing segments relative to the rim (the torque is independent of γ) and therefore the three linear bearings may be treated as two rotational bearings. The bearing torques can now be written as

$$\left.\begin{aligned} T_{ax} &= -K_\lambda(\phi_a - \phi_s) - K_\lambda^{\cdot}\left(\dot{\phi}_a - \dot{\phi}_s\right) - K_\lambda^{\cdot}\dot{\delta}(\theta_a - \theta_s) \\ T_{ay} &= -K_\lambda(\theta_a - \theta_s) - K_\lambda^{\cdot}\left(\dot{\theta}_a - \dot{\theta}_s\right) + K_\lambda^{\cdot}\dot{\delta}(\phi_a - \phi_s) \end{aligned}\right\} \quad \text{(C18)}$$

The spin motor torque can be used to control either spacecraft Z-axis attitude or attitude rate as well as to counteract rim drag torque (hysteresis and eddy current losses). In this derivation the component of motor torque which is greater than the drag torque is of interest and

$$T_{az} = T_c - T_d \quad \text{(C19)}$$

where the subscripts c and d refer to control and drag.

Note that

$$T_s = -E_{sa}T_a \quad \text{(C20)}$$

Thus, equations (C10) to (C12) and (C17) to (C20) represent the nonlinear AMCD-spacecraft "passive" case equations of motion.

These equations can be linearized by assuming small angular motions except about the spin axis, and for the case where $T_c = T_d$ and $G = 0$, they become

$$\left.\begin{aligned} I_a\ddot{\phi}_a &= -K_\lambda(\phi_a - \phi_s) - K_\lambda^{\cdot}(\dot{\phi}_a - \dot{\phi}_s) - H_{az}\dot{\theta}_a - K_\lambda^{\cdot}\dot{\delta}(\theta_a - \theta_s) \\ I_a\ddot{\theta}_a &= -K_\lambda(\theta_a - \theta_s) - K_\lambda^{\cdot}(\dot{\theta}_a - \dot{\theta}_s) + H_{az}\dot{\phi}_a + K_\lambda^{\cdot}\dot{\delta}(\phi_a - \phi_s) \\ I_s\ddot{\phi}_s &= K_\lambda(\phi_a - \phi_s) + K_\lambda^{\cdot}(\dot{\phi}_a - \dot{\phi}_s) - H_{sz}\dot{\theta}_s + K_\lambda^{\cdot}\dot{\delta}(\theta_a - \theta_s) \\ I_s\ddot{\theta}_s &= K_\lambda(\theta_a - \theta_s) + K_\lambda^{\cdot}(\dot{\theta}_a - \dot{\theta}_s) + H_{sz}\dot{\phi}_s - K_\lambda^{\cdot}\dot{\delta}(\phi_a - \phi_s) \end{aligned}\right\} \quad \text{(C21)}$$

where

$$H_{sz} = I_{sz}\dot{\delta}$$

$$H_{az} = I_{az}\dot{\xi}$$

The linearized equations for the Z-axis represent simple single-axis reaction-wheel dynamics and are not considered.

REFERENCES

1. Notti, J. E.; Cormack, A., III; and Schmill, W. C.: Integrated Power/Attitude Control System (IPACS) Study. Vol. I – Feasibility Studies. NASA CR-2383, 1974.

2. Lawson, Louis J.: Design and Testing of High Energy Density Flywheels for Application to Flywheel/Heat Engine Hybrid Vehicle Drives. 1971 Intersociety Energy Conversion Engineering Conference, Soc. Automot. Eng., Inc., c.1971, pp. 1142-1150.

3. Jacot, A. Dean; and Emsley, William W.: Assessment of Fine Stabilization Problems for the LST. AIAA Paper No. 73-881, Aug. 1973.

4. Anon.: Proceedings of the Symposium on Attitude Stabilization and Control of Dual-Spin Spacecraft 1-2 August 1967. Rep. No. SAMSO-TR-68-191, U.S. Air Force, Nov. 1967. (Available from DDC as AD 670 154.)

5. Flatley, Thomas W.: Equilibrium States for a Class of Dual-Spin Spacecraft. NASA TR R-362, 1971.

6. Mingori, D. Lewis: Stability of Linear Systems With Constraint Damping and Integrals of the Motion. Astronaut. Acta, vol. 16, no. 5, Nov. 1971, pp. 251-258.

7. Anon.: Research and Applications Modules (RAM) Phase B Study. Rep. No. GDCA-DDA 72-007 (Contract NAS 8-27539), General Dynamics Corp., May 12, 1972. (Available as NASA CR-123785.)

8. Anderson, Willard W.: On Lateral Cable Oscillations of Cable-Connected Space Stations. NASA TN D-5107, 1969.

NASA-Langley, 1975 L-9901